Proceedings of the Pakistan Academy of Sciences:
A. Physical and Computational Sciences: 57 (2): 51-74 (2020)

ISSN: 2518-4245 (print), 2518-4253 (online)

Pakistan Academy of Sciences

Research Article

Effect of Molarity on the Structure, Optical Properties, and Surface Morphology of (002)-Oriented Ni_2O_3 Thin Films Deposited via Spray Pyrolysis

Muzamil Aftab[1], Muhammad Zakria Butt[1*], Dilawar Ali[2], Muhammad Usman Tanveer[1], and Ali Hussnain[2,3]

[1]Centre for Advanced Studies in Physics, GC University Lahore-54000, Pakistan
[2]Department of Physics, GC University Lahore-54000, Pakistan
[3]Department of Physics, Minhaj University, Township Campus, Lahore-54770, Pakistan

Abstract: Ni_2O_3 thin films with seven molar concentrations in the range 0.01 – 0.5 M were deposited on pre-heated glass substrates employing spray pyrolysis technique. Structure of the films was (002) oriented hexagonal. The peak intensity and crystallite size increased exponentially with the increase in molarity. Both uniform and non-uniform lattice strains as well as stacking fault probability decreased linearly on increasing molarity. Average values of optical absorbance (0.554 – 0.762), extinction coefficient (0.285 – 0.391), and optical conductivity (2.43 – 3.02) in the visible region (λ = 380 – 740 nm) increased rapidly with molarity in the low molarity range 0.01 – 0.05M and rather slowly in the high molarity range (0.1 – 0.5 M). Both direct (3.99 – 4.045 eV) and indirect (3.37 – 3.52 eV) band gaps decreased whereas Urbach energy (0.33 – 0.42 eV) increased on increasing molarity. Optical reflectance of the films (λ = 270 – 900 nm) was less than 10%. Average reflectance (4.677 – 5.774 %) in the visible region (λ = 380 – 740 nm) decreased linearly on increasing molarity. The average refractive index (1.33 – 1.53) in the visible region decreased linearly with increase in molarity. Surface morphology of the films consisted of random shape nanoparticles. Average surface roughness of the films (0.173 – 0.366 μm) increased rapidly with molarity in the range 0.01 – 0.03 M, and then decreased to an intermediate level (0.284 μm) around which it undulated in the range 0.05 – 0.5 M. Surface roughness of the films strongly exerted its influence on the absorbance, extinction coefficient, and optical conductivity of the films.

Keywords: Spray pyrolysis, Ni_2O_3 thin films, X-ray diffraction, Surface morphology, Optical properties

1. INTRODUCTION

Optical transparency and electrical conductivity are two most important properties of ceramics, metals and semiconductors. It is very difficult for a material to possess both of them simultaneously. However, there are some metallic oxides, called transparent conducting oxides, that possess combination of both, i.e. their optical transparency is above 85% in the visible region besides electrical conductivity close to the metallic conductivity (~104 Scm^{-1}). Due to such unique properties, they have a large number of applications in emerging technologies [1 – 5]. Among various transparent conducting oxides, the oxides of nickel (NiO, Ni_2O_3) are reported to have a large number of applications. NiO is well characterized p-type semiconductor having band gap in the range 3.6 ─ 4.0 eV, and can therefore be opted in designing photodetectors [6], smart windows [7], UV detector [8], dye sensitized solar cells [9], and gas sensors [10]. Ni_2O_3, which is also called Nickel (III) oxide as per IUPAC classification or black nickel oxide, is not that much characterized as NiO but it has been used in combination with other materials for various purposes [11 – 17].

Wen et al. [11] have investigated the influence of Ni_2O_3 and carbon black as a joint catalyst for the carbonization of polystyrene, polyethylene, polypropylene and their blends. They found that

Received: March 2020; Accepted June 2020
*Corresponding Author: Muhammad Zakria Butt <mzakriabutt@gmail.com>

the combination of these compounds was efficient in producing good quality carbon nanotubes with high yields and catalyzing carbonization of these polymers. Similarly, Dey et al. [12, 13] have used NiO, Ni_2O_3 and Cu doped Ni oxide (CuxNi1-xO) as sensing material to sense the Cr(VI) toxic ions in aqueous medium. They reported that Ni_2O_3 have superb Cr(VI) adsorption capacity; it adsorbs nearly 60% Cr(VI) during 3 hours from the aqueous solution. Likewise, Chen et al. [14, 15] have reported that Ni_2O_3 is a good electrochromic material having wide transmittance contrast between coloring and bleaching state in the visible light range. So it may be employed in the fabrication of non-linear optic devices. Hu et al. [16] have found that Ni_2O_3 helped in the degradation of 2, 4, 6-Trichlorophenol by improving the photocatalytic action of the composite photocatalyst N-TiO2 within visible light range. They also found that with the usage of Ni_2O_3, the composite photocatalyst was much more stable than the catalyst alone. Similar response has been observed by Zhao et al. [17] who investigated the photocatalytic activity using the B doped TiO2 loaded with Ni_2O_3. Their findings suggested that photocatalytic activity is enhanced greatly with the incorporation of Ni_2O_3 and toxic organic pollutants can be degraded to a greater extent easily. These applications make Ni_2O_3 an interesting candidate for material research.

Literature survey shows that various routes are adopted in order to synthesize and grow nickel oxide thin films, e.g. electroless method [14], chemical deposition [15], chemical spray pyrolysis [18, 19], radio frequency magnetron sputtering [20], and sol-gel spin coating [21]. All these methods have different advantages depending upon their applications and to obtain the films with desired properties. Among them, spray pyrolysis is a relatively simple, inexpensive, and easy way to grow thin films [22, 23]. By this method, one can cover rather large area and prepare films for optoelectronic devices [24].

No systematic studies have been made so far pertaining to the impact of molarity on the characteristics of Ni_2O_3 thin films. In the present work, Ni_2O_3 thin films have been deposited on pre-heated glass substrates using spray pyrolysis technique, and their optical, structural, and morphological properties have been investigated vis-à-vis molarity over the wide range of 0.01 – 0.5 M. Since Ni_2O_3 is not a well characterized oxide of nickel, so the results obtained in this work may provide better understanding of Ni_2O_3, which will be helpful in designing Ni_2O_3 based devices.

2. EXPERIMENTAL DETAILS

2.1 Deposition of Ni_2O_3 Thin Films

Chemical spray pyrolysis method was employed for growing Ni_2O_3 thin films using glass as substrate which was heated to 250°C. High purity nickel acetate tetra-hydrate ($Ni(CH_2COO)_2 \cdot 4H_2O$) was dissolved in 2-methoxtethanol ($C_3H_8O_2$) to prepare 0.5 M stock solution. The mixture was then stirred at a rate of 100 rpm for 2 hours at 60° C. During stirring, stabilizer monoethanolamine (C_2H_7NO) was added drop by drop into the solution. After stirring, bluish green colored homogeneous and clear solution was obtained. From the clear stock solution, the spray solutions with different molarities (0.01, 0.03, 0.05, 0.1, 0.2, 0.3, and 0.5 M) were prepared. Before spraying, cleaning of glass substrates was done in ultrasonic bath with deionized water followed by rinsing in acetone and then heating to a temperature of 250°C. The solution was then sprayed using a perfume atomizer. The advantages of using a perfume atomizer are that (i) fine atomization can be done, (ii) no carrier gas is required, and (iii) intermittent spraying is possible [25]. Spray process was optimized at the following conditions: distance between atomizer and substrate = 30 cm, spray rate = 0.2 mL/min, and interval between successive sprays = 1.5 min. After deposition, the Ni_2O_3 thin films were annealed in air for 2 h at 300 °C.

2.2 Characterization of Ni_2O_3 Thin Films

X-ray diffractrometer (X' pert PANalytical) with Cu-Kα radiations source was employed to investigate the structure of Ni_2O_3 thin films with various molarities. X-ray diffraction (XRD) pattern was recorded for each film over the 2θ range 20° – 80°. The scan speed, operating current, and operating voltage were 0.1°/s, 40 mA, and 40 kV, respectively. Scanning electron microscope (JEOL JSM-6480 LV) was employed to examine the morphology of the film surface. To evaluate their optical properties, UV–VIS–NIR

spectrophotometer (Cary 60 Agilent Technology) was utilized.

3. RESULTS AND DISCUSSION

3.1 Structural Analysis

3.1.1 XRD Patterns

TDiffractographs obtained for Ni_2O_3 thin films with molarities in the range 0.01 ─ 0.5 M have been presented in Fig. 1. All them match fairly well with the JCPDS card number 00-014-0481 confirming hexagonal structure of the films with one major peak of (002) plane [26]. However, peak of (004) plane also appeared but only for molar concentration of 0.5 M. One can note that the change in molarity has not induced any new phase in the specimens. Moreover, one can see that for rather small values of molarities, i.e. 0.01 ─ 0.05 M, the peaks are not sharp and well defined in shape. But for higher molarities in the range 0.1 ─ 0.5 M, the peaks become sharp and well defined indicating improved crystallinity. The values of peak intensity pertaining to (002) plane, given in Table 1, are represented by squares in Fig. 2a vis-à-vis molarity. The curve fitted to the data points by means of least-squares fitting method (Sigmoidal Boltzmann Model), displays

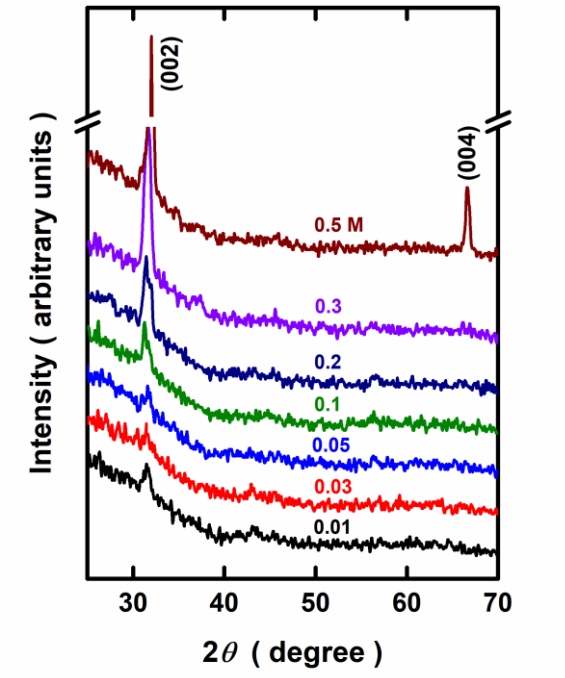

Fig 1. XRD patterns of Ni_2O_3 thin films for molarities ranging from 0.01 to 0.5 M.

that the peak intensity is increasing exponentially as molarity increases, which means that crystallinity improves as the molarity of the films increases [27, 28]. Mathematically, this behavior is encompassed by the expression:

$$I = \frac{A_1 - A_2}{1 + e^{(M - M_O)/dM}} + A_2 \qquad (1)$$

where A_1= 88.3, A_2 = 4595, M_o = 0.667, and dM = 0.667, with correlation factor r^2 = 0.999.

3.1.2 Crystallite Size

To measure the crystallite size (D), one can make use of well-known Sherrer equation [29, 30]:

$$D = \frac{k\lambda}{\beta cos\theta} \qquad (2)$$

where β (in radian) is full width at half maximum (FWHM) of the diffraction peak, θ is the corresponding Bragg angle, k is shape factor (≈ 0.94), and λ is X-rays wavelength (0.15406 nm for Cu Kα). The values of D obtained by Sherrer equation have been presented in Table 1. Now, symbols in Fig. 2b denote the values of peak intensity vis-à-vis crystallite size. The curve passed through the data points by statistical method referred to above shows that peak intensity increases exponentially with the increase in crystallite size (D). Mathematically, it is represented by the equation:

$$I = 51.24exp\left(\frac{D}{9}\right) \qquad (3)$$

with correlation factor r^2 = 0.997. It confirms that as crystallinity increases peak intensity also increases and vice versa.

Since intensity of the diffraction peak (002) increases exponentially with both molarity and crystallite size (Fig.2a and Fig.2b), a linear relationship between crystallite size and molarity cannot be ruled out. This has been demonstrated in Fig 2c. Using least-squares fitting method, a straight line has been drawn through the data points, which is mathematically encompassed by the equation:

$$D = 3.43 + 36.40\ M \qquad (4)$$

with linear correlation coefficient r = 0.937. Such linear relationship between crystallite size and

Table 1. Structural data pertaining to (002) crystallographic plane.

Molarity	*I* (cps)	*D* (nm)	Strain (Wilson Formula)	Strain (Peak Shift)	SFP
0.01	95	5.55	0.0240	0.0141	0.4032
0.03	87	4.69	0.0285	0.0139	0.3961
0.05	93	4.82	0.0277	0.0142	0.4058
0.1	110	8.98	0.0150	0.0214	0.6065
0.2	129	8.16	0.0164	0.0151	0.4315
0.3	188	10.68	0.0124	0.0086	0.2458
0.5	777	24.48	0.0054	-0.0022	0.0637

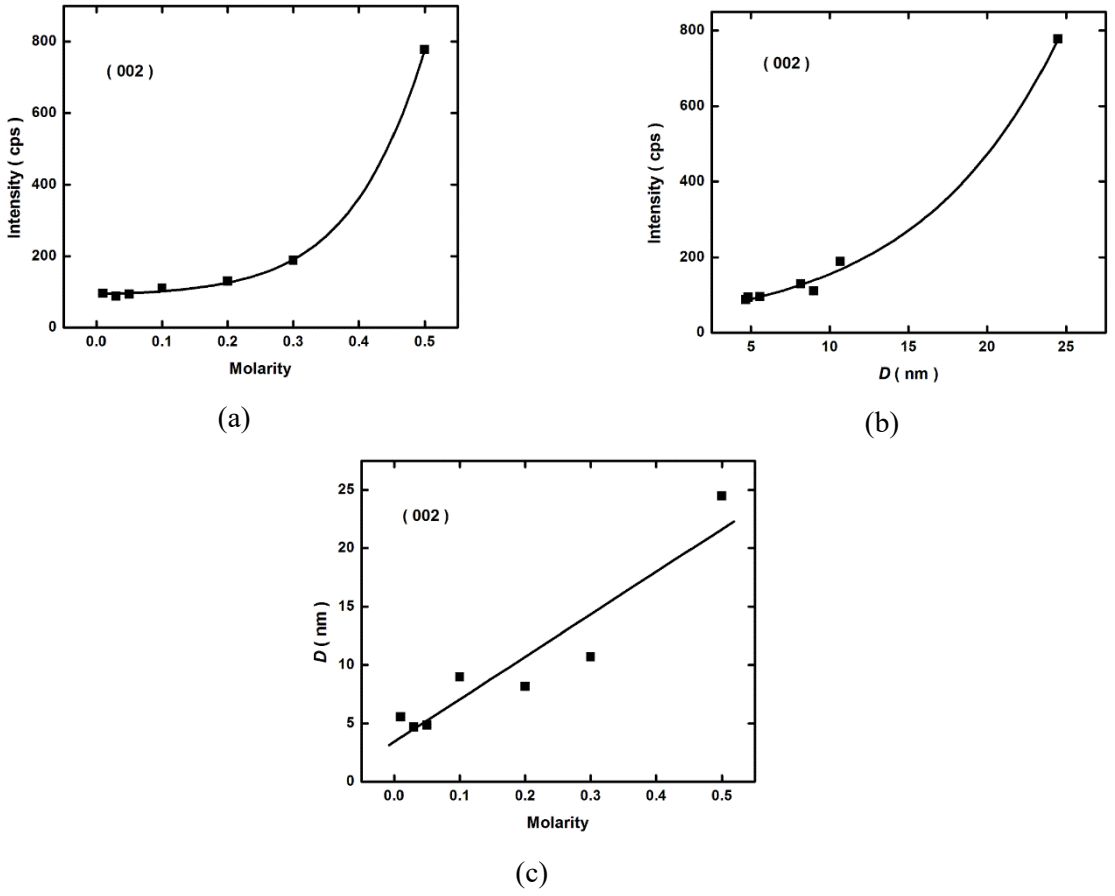

Fig 2. Diffraction peak intensity of (002) plane of Ni_2O_3 thin films as a function of (a) molarity and (b) crystallite size *D*. (c) Correlation between intensity and crystallite size for (002) plane.

molarity, has also been affirmed previously by Bakr et al. [18] for $Ni_{0.92}Co_{0.08}O$ thin films.

3.1.3 Lattice Strain

Strain is generally defined as the deformation in a specimen in terms of relative displacement of its particles from their original positions. The deformation may be due to changes in temperature, chemical reactions or external loads on the body. As a result of deformation, strain will be induced which may be uniform or non-uniform. Uniform strain may slightly shift the diffraction peak from its original position and non-uniform strain will broaden the peaks [29].

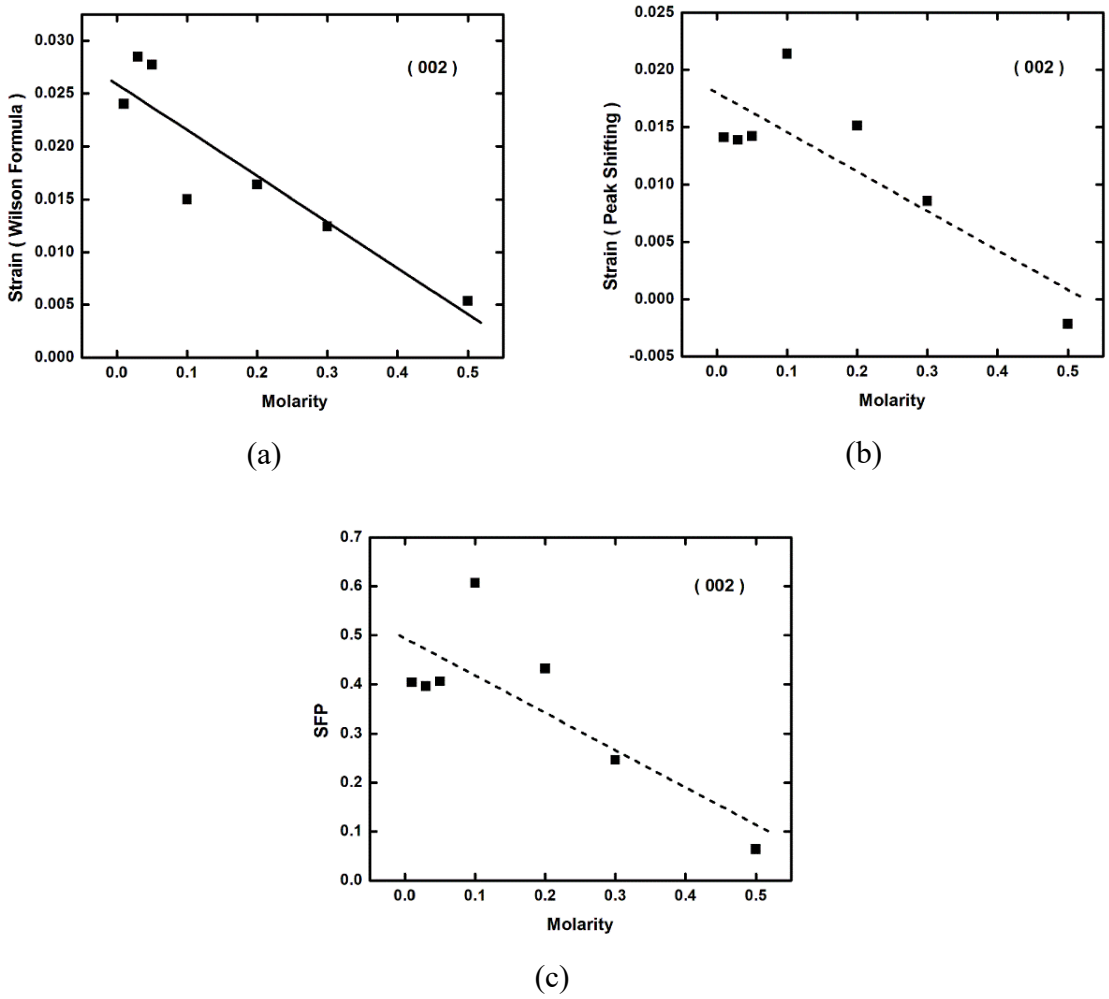

Fig 3. Strain calculated by Wilson formula (a) and from the peak shifting (b) of (002) plane as a function of molarity. (c) Stacking Faults Probability (SFP) for (002) plane as a function of molarity.

In this work, we have studied both types of strains induced in the Ni_2O_3 thin films of different molarities. To calculate the non-uniform strain causing peak broadening, Wilson formula [27] has been used, which is given as under:

$$\text{Strain (WF)} = \varepsilon = \frac{\beta cot\theta}{4} \qquad (5)$$

The obtained values of the non-uniform strain, given in Table 1, are symbolized by squares in Fig. 3a vis-à-vis molarity. Note that the non-uniform strain is decreasing with the increase in molarity. A straight line statistically passed through the data points is mathematically given as under:

$$\text{Strain (PB)} = 0.0259 - 0.0435M \qquad (6)$$

with linear correlation coefficient r = — 0.906. So, the non-uniform strain, which causes peak broadening, decreases linearly with the increase in molarity.

On the other hand, peak shift approach assumes that, if the crystallites are in the state of strain then the d- spacing will be changed from d to $d \pm \delta d$, and as a result the peak position changes from 2θ to $(2\theta \pm 2\delta\theta)$. In this method uniform strain can be calculated using the relation:

$$\text{Strain (PS)} = \varepsilon = \frac{\Delta d}{d} = \left(\frac{d_i - d_u}{d_u}\right) \qquad (7)$$

where d_u is the standard value of d-spacing for crystallographic plane (002) [26] and di is the value of d-spacing for crystallographic plane (002) in a thin film of a given molarity. The calculated values for uniform strain, given in Table 1, are symbolized by squares in Fig 3a & 3b vis-à-vis molarity. A straight line passed through the data points is mathematically given as under:

$$\text{Strain (PS)} = 0.0179 - 0.0343M \quad (8)$$

with linear correlation coefficient r = -0.834.
One can therefore infer that as molarity is increased, the uniform strain in the thin films is also reduced like the non-uniform strain referred above.

3.1.4 Stacking Fault Probability

Another important factor that might influence the crystallinity of the films is stacking fault probability (SFP) [31, 32], which can be calculated by the formula:

$$SFP = \left[\frac{2\pi^2}{45\sqrt{3}}\right]\left[\frac{\Delta 2\theta}{tan\theta}\right] \quad (9)$$

where Δ2θ is the shift in the peaks with respect to the peak position in the reference pattern. The values of SFP for (002) plane obtained by means of above expression are listed in Table 1. In Fig. 3c squares symbolize the SFP values as a function of molarity. One can see that SFP is decreasing with the increase in molarity which in turn results in the enhancement of crystallinity. This trend is embodied by the relation:

$$\text{SFP} = 0.494 - 0.759M \quad (10)$$

with linear correlation coefficient r = -0.801.

3.2 Optical Analysis

3.2.1 Optical Absorbance

The optical absorbance of Ni_2O_3 thin films of various molarities has been studied for 270 – 900 nm wavelengths. The recorded absorbance spectra are given in Fig 4a. One can see that absorbance is increased as molarity increases. Balu et al. [33] have also found the same response for NiO thin films with various molar concentrations. They attributed this response to the size of clusters containing nano grains formed on the surface; higher the molar concentration bigger the size of clusters. Other factors that may affect the optical absorbance include density of defect states, band gap, and thickness of the films [34]. A worth noting point is that for all the molarities, absorbance is very high in the UV region whereas in visible and near IR region it is fairly low. This behavior can be attributed to the fact that the photons in UV region are rather energetic. Electrons from the valence band are therefore excited to the conduction band due to absorption of these energetic photons. On the other hand, photons in visible and IR regions are rather less energetic and their interaction with atoms is not strong enough to get fully absorbed and are eventually transmitted [35]. Dependence of average absorbance in visible region (380 – 740 nm), listed in Table 2, on molarity of Ni_2O_3 thin films is portrayed in Fig 4b.

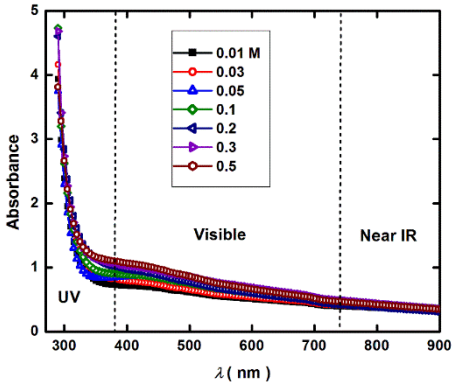

(a)

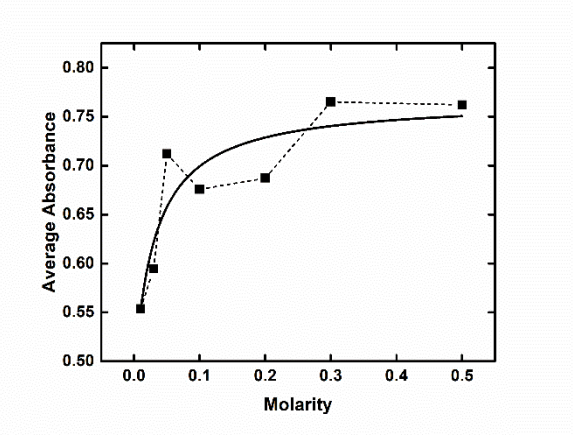

(b)

Fig 4. (a) Absorbance spectra of Ni2O3 thin films of various molarities in the wavelength range 270 – 900 nm. (b) Variation in the average absorbance of Ni_2O_3 thin films in the visible region as a function of molarity.

An exponential fit to the data points is mathematically given by:

$$A_{ave} = \exp[\frac{a+b}{M+c}] \quad (11)$$

with a = -0.265, b = -0.012, and c = 0.025.

The correlation factor r^2 = 0.858 is reasonably close to 1. One can see that average absorbance in

Table 2. Optical characteristics of Ni_2O_3 films in visible region.

Molarity	Average Absorbance	Average Reflectance (%)	Average Extinction Coefficient (k)	Average Refractive Index (n)	Average Optical Conductivity (×1015)
0.01	0.554	5.542	0.285	1.525	2.43
0.03	0.595	5.774	0.305	1.529	2.62
0.05	0.712	5.739	0.367	1.468	3.02
0.1	0.676	5.345	0.346	1.455	2.84
0.2	0.687	5.377	0.349	1.456	2.89
0.3	0.765	4.906	0.391	1.353	2.99
0.5	0.762	4.677	0.387	1.333	2.92

the visible region increases rapidly with molarity in the low molarity range (0.01 – 0.05 M) and slowly in the high molarity range (0.1 – 0.5 M).

3.2.2 Optical Band Gap

Optical band gap (Eg) pertaining to Ni_2O_3 films can be evaluated using Tauc relation [36]:

$$\alpha h\upsilon = \beta\,(h\upsilon - E_g)^m \qquad (12)$$

where $\alpha = (= (2.303\,A)/t)$ is absorption coefficient, A is absorbance, t (≈ 1.924 μm) is thickness of the film, υ is photon frequency, h is Planck's constant , and β is a constant called band edge parameter. The transition process, whether it is direct or indirect, is determined by the parameter m. For direct band gap (DBG), m = 1/2 while for indirect band gap (IBG), m = 2 [37 ─ 39]. Regarding the energy band gap in NiO thin films, some authors report both direct and indirect band gaps [40, 41] while others evaluate only indirect band gap [42 – 46]. However, we will determine both direct as well as indirect band gap for Ni_2O_3 thin films. The parameter $(\alpha h\upsilon)^2$ has been depicted by symbols in Fig 5 vis-à-vis photon energy ($h\upsilon$) for direct band gap transitions, whereas the parameter $(\alpha h\upsilon)^{1/2}$ has been depicted by symbols in Fig 6 vis-à-vis photon energy ($h\upsilon$) for indirect band gap transitions. On extrapolation of the linear portion of a plot to $h\upsilon$ – axis for $(\alpha h\upsilon)^2 = 0$ and $(\alpha h\upsilon)^{1/2} = 0$, the values of DBG and IBG for each of the films were determined (Table 2). The points in Fig 7 represent the values of DBG and IBG as a function of molarity.

The straight lines fitted to the data points in Fig 7 in each case are given by the expressions:

$$E_g^{\mathrm{D}} = 4.034 - 0.063\mathrm{M} \qquad (13)$$

$$E_g^{\mathrm{ind}} = 3.506 - 0.217\mathrm{M} \qquad (14)$$

with linear correlation coefficient r = - 0.616 and - 0.735, respectively. Thus as molarity of Ni_2O_3 thin film increases, the energy band gap Eg decreases.

Mahmoud et al. [47] have also observed such decreasing trend in the band gap of NiO thin films as their molarity is increased. They attributed this behavior to enhancement in degree of crystallinity of the films. However, according to Anwar and Hogarth [48], oxygen ion vacancies may also cause reduction in band gap; these positively charged vacancies may capture some free electrons and act as donor centers leading to the reduction in band gap.

3.2.3 Urbach Energy

Urbach energy (Eu) is basically related to the disorder or concentration of defects states in the thin films, which perturb the structure of their energy band [49, 50]. Eu for Ni_2O_3 thin films of various molarities has been calculated by using the empirical relation [51]:

$$\alpha = \alpha_o e^{\left(\frac{h\upsilon}{E_u}\right)} \qquad (15)$$

where α_o is pre-exponential constant which depends upn material and α is the absorption coefficient. It is evaluated by plotting $\ln\alpha_o$ vis-à-vis hυ as illustrated in Fig 8. Numerically, Eu is equal to the inverse slope of the linear portion of lnα_o- hυ plot. Table 3 presents Eu values, which have been depicted by squares vis-à-vis molarity in Fig 9. A linear fit made to the data points is mathematically

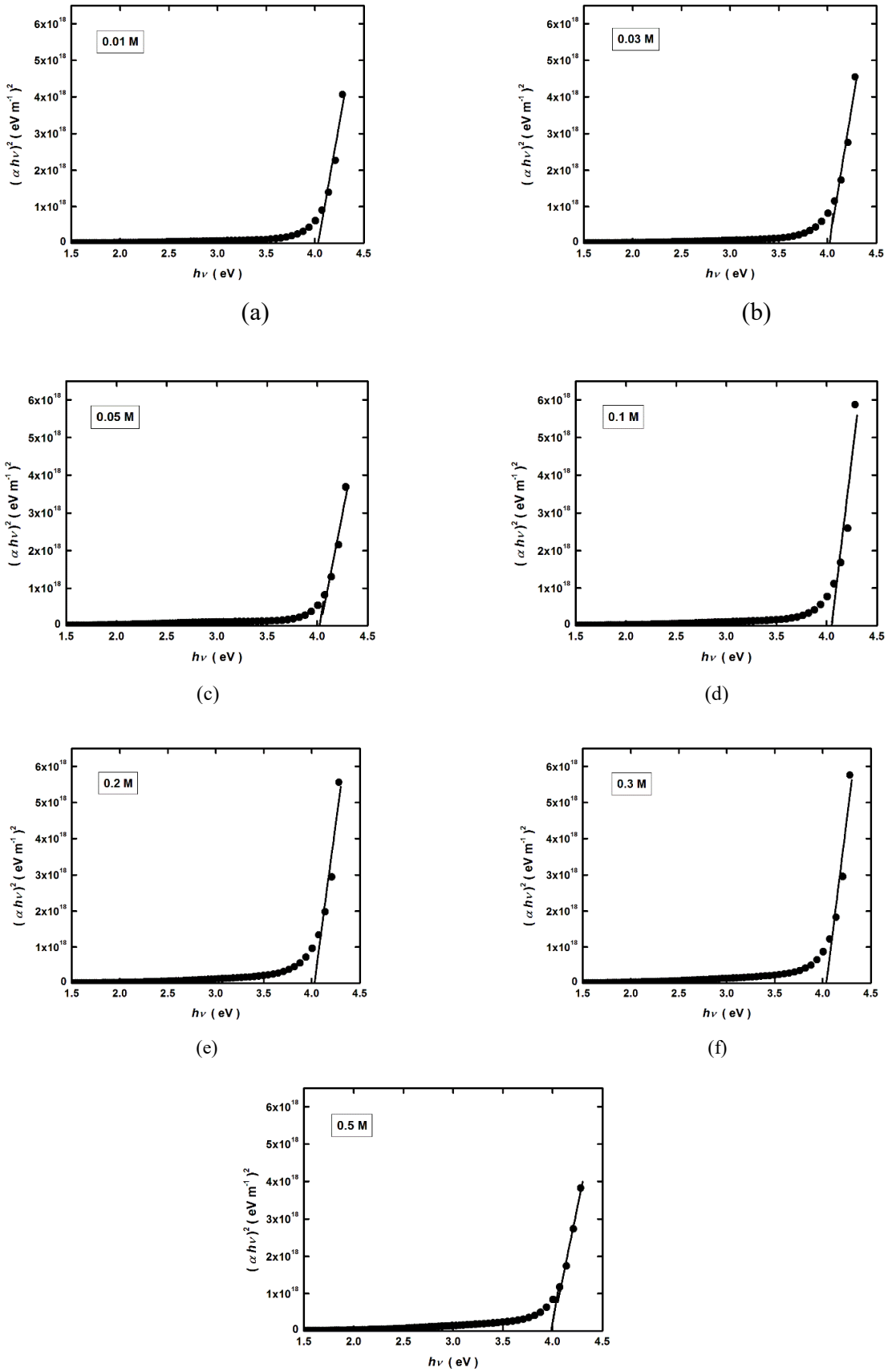

Fig 5. Evaluation of the direct band gap in Ni_2O_3 thin films of different molarities.

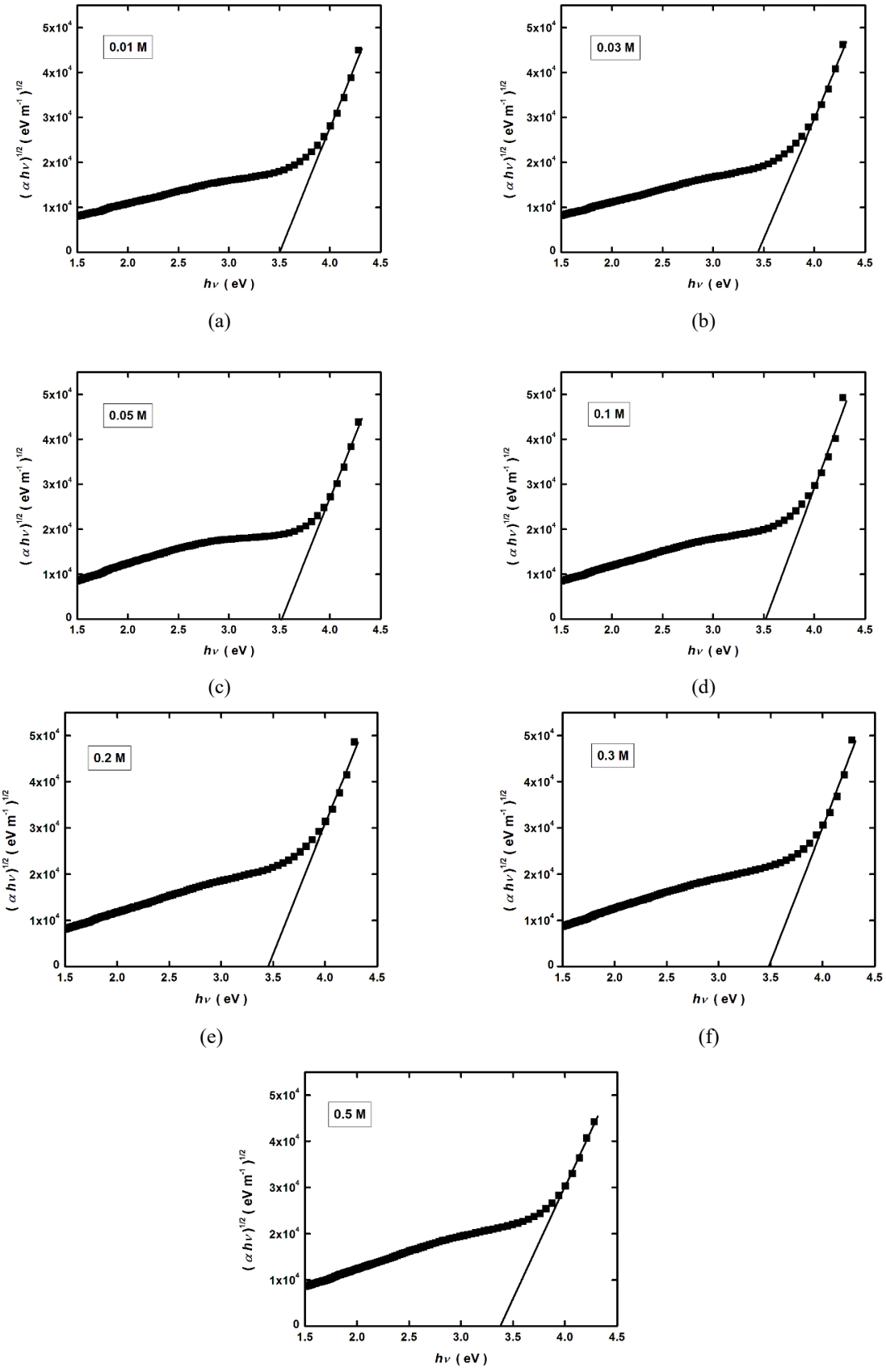

(a) (b) (c) (d) (e) (f) (g)

Fig 6. Evaluation of the indirect band gap in Ni2O3 thin films of different molarities.

Table 3. Bandgap and Urbach Energy of Ni_2O_3 films.

Molarity	Direct Bandgap (eV)	Indirect Bandgap (eV)	Urbach Energy (eV)
0.01	4.029	3.501	0.345
0.03	4.015	3.446	0.377
0.05	4.028	3.516	0.334
0.1	4.045	3.520	0.345
0.2	4.023	3.444	0.393
0.3	4.035	3.487	0.366
0.5	3.988	3.372	0.423

represented as below:

$$Eu = 0.3452 + 0.1399M \quad (16)$$

with linear correlation coefficient r = 0.794. An increasing trend of Urbach energy with increasing molarity of the films is evident. Such behavior has also been observed by many researchers [52 – 54].

3.2.4 Optical Band Gap versus Urbach Energy and Crystallite Size

Figure 10a portrays the dependence of optical band gap E_g on Urbach energy E_u. Linear fit to the data point is represented mathematically by the relations:

$$E_g^D = 4.199 - 0.477E_u \quad (17)$$

$$E_g^{ind} = 4.073 - 1.635E_u \quad (18)$$

with linear correlation coefficient r = - 0.789 and - 0.969, respectively. Thus an inverse relation can be seen between E_g and E_u. This trend was also observed by many authors for NiO and different materials as well [55 – 59]. Similarly, Fig 10b demonstrates the dependence of optical band gap E_g on crystallite size D. An inverse relation is evident between the two parameters. The following equations:

$$E_g^D = 4.041 - 0.0018D \quad (19)$$

$$E_g^{ind} = 3.525 - 0.0058D \quad (20)$$

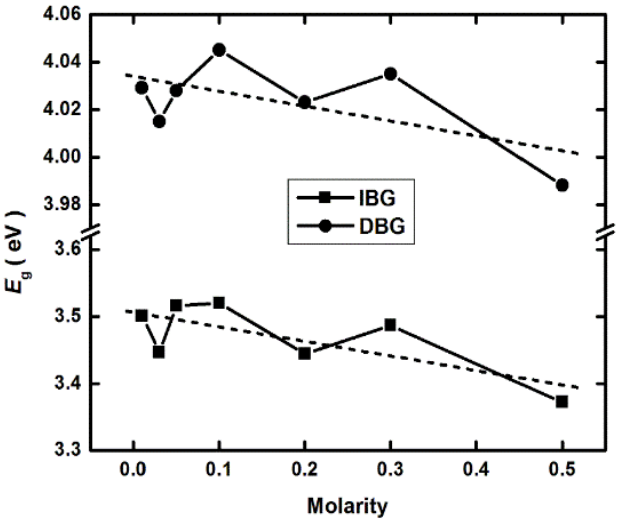

Fig 7. Values of direct and indirect band gaps of Ni_2O_3 thin films as a function of molarity.

with linear correlation coefficient r = - .702 and -0.757, respectively represent the straight lines passed through the data points This trend is attributed to the improvement in crystallinity, which results in the reduction of optical band gap [47].

3.2.5 Optical Reflectance

The optical reflectance data (wavelength range = 270 – 900 nm) of Ni_2O_3 films synthesized in the present work have been portrayed in Fig 11a. It can be readily seen that optical reflectance is far less than 20% which means that the films are transparent [60]. In Fig 11b, average reflectance in the visible region (380 – 740 nm) has been plotted against molarity. A linear fit to the data points is encompassed by following expression:

$$R_{ave} = 5.706\text{-}2.173M \quad (21)$$

with linear correlation coefficient r = — 0.942. One can see that average reflectance is reducing as the molarity of the films is increasing. Additionally, the values of the average reflectance are rather low which indicate that these films can behave as antireflection films. Vigneshkumar et al. [61] have prepared antireflection thin film of NiO for its use in solar cells employing spray pyrolysis technique. They calculated a reflectance of 7 % at the wavelength of 550 nm, and suggested that it can be successfully used as antireflection film in solar cells.

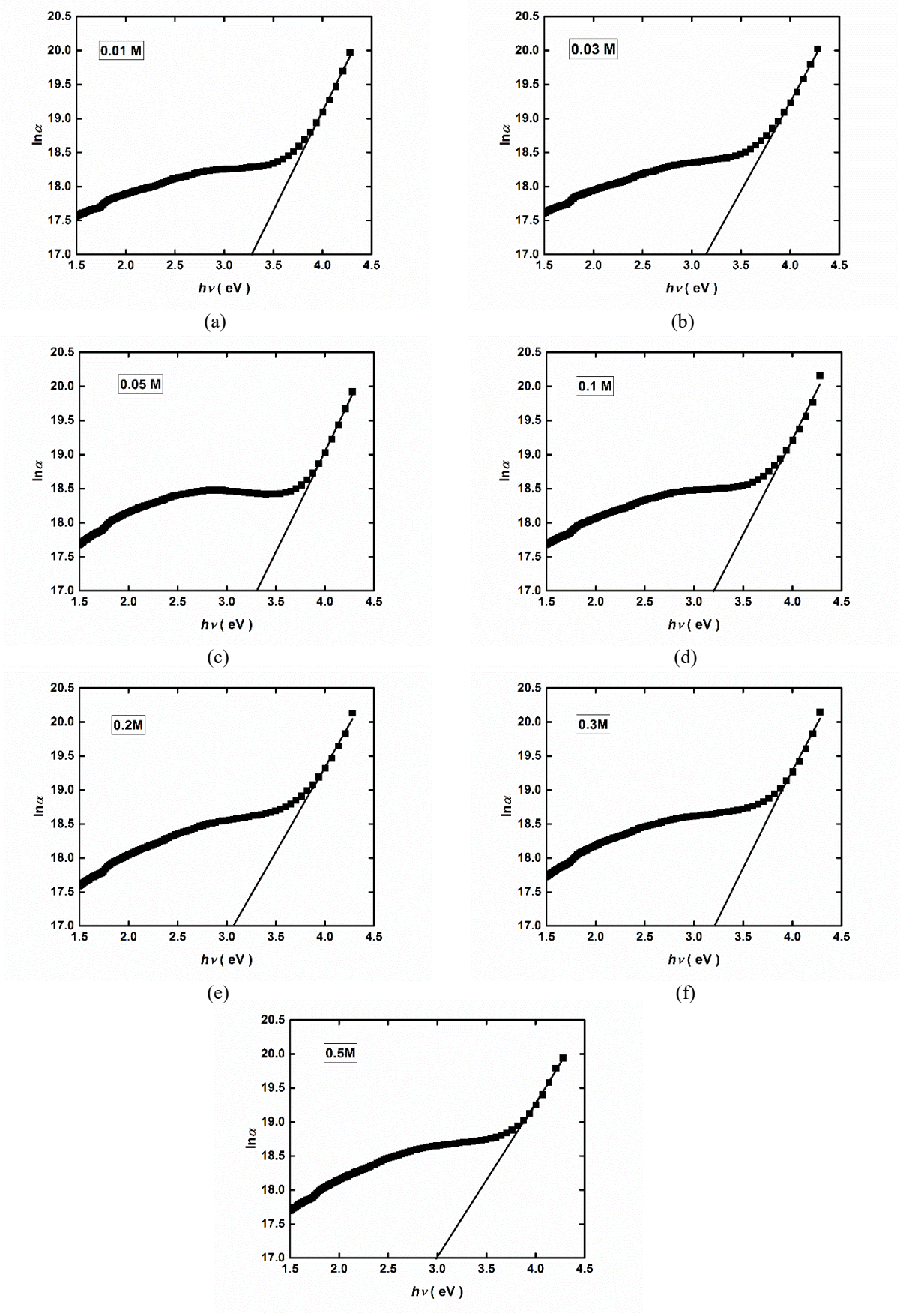

Fig 8. Plots for evaluation of Urbach energy in Ni2O3 thin films of different molarities.

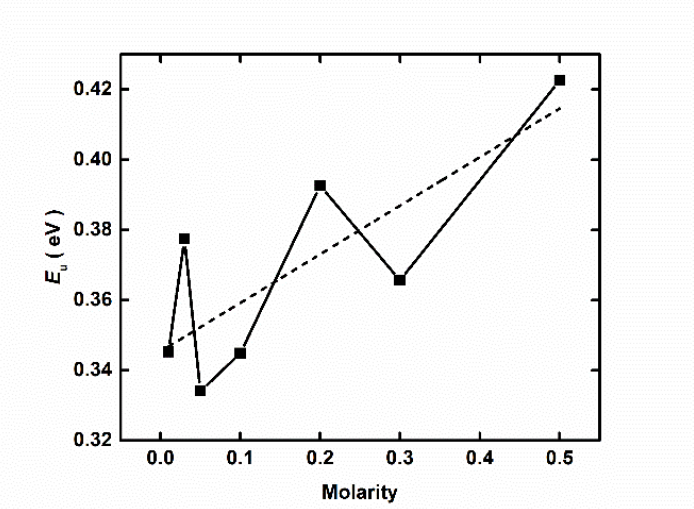

Fig 9. Values of Urbach energy in Ni_2O_3 thin films as a function of molarity.

3.2.6 Refractive Index and Extinction Coefficient

Refractive index (n) is an important dimensionless optical constant of a material which articulates about propagation of electromagnetic waves through the medium. It depends on the wavelength λ of light propagating through the medium. During the propagation of light through a lossy medium, it undergoes attenuation and dispersion; its energy is lost in the processes of scattering, photo-generation, generation of lattice waves, etc. [20]. As a consequence, n becomes a complex number $n^* = n + ik$ [20, 62]. Here k is called extinction coefficient or absorption index. The complex refractive index, n^* can be determined using the relations [20, 51, 62]

$$n = \left(\frac{1+R}{1-R}\right) + \sqrt{\frac{4R}{(1-R)^2} - k^2} \qquad (22)$$

$$k = \frac{\alpha\lambda}{4\pi} \qquad (23)$$

where R is the reflectance of the medium.

The measured values of extinction coefficient k of Ni_2O_3 thin films of various molarities have been plotted against wavelength λ (270 – 900 nm) in Fig. 12a. Variation of k with λ is almost identical for all the molar concentrations of Ni_2O_3 thin films. Moreover, the average values of k in the visible region (380 – 740 nm) as a function of molarity are given in Fig 12b. An exponential fit to the data points is mathematically given by:

$$k_{ave} = \exp[\frac{a+b}{M+c}] \qquad (24)$$

with a = -0.944, b = -0.010, and c = 0.022. The correlation factor r^2 = 0.834 is reasonably close to 1. One can see that average extinction coefficient in the visible region increases rapidly with molarity in the low molarity range (0.01 – 0.05M) and slowly in the high molarity range (0.1 – 0.5M). The reason for such a trend can be attributed to the fact that extinction coefficient (k) is proportional to absorption coefficient (α) of the films (Eq. (23) and absorbance of the films is increasing with the increase in molarity (Fig 4b).

The refractive index n has been presented in Fig. 13a vis-à-vis the wavelength λ for the entire set of Ni_2O_3 films. It can be seen that refractive index decreases with wavelength in a similar manner for each film. One can also note that as molarity increases refractive index decreases. The decline in the refractive index values towards longer wavelength may be attributed to the effect of lattice absorption [24].

Moreover, the squares in Fig. 13b denote average refractive index values in the visible region (380 – 740 nm) vis-à-vis molarity. The mathematical expression given below represents the correlation between these two parameters:

$$n_{ave} = 1.514 - 0.401M \qquad (25)$$

with linear correlation coefficient $r = -0.934$.

3.2.7 Optical Conductivity

The term optical conductivity σ_op may be defined as the conductivity which arises in the presence of optical excitation without the presence of applied electrical field [63]. It can be estimated using the

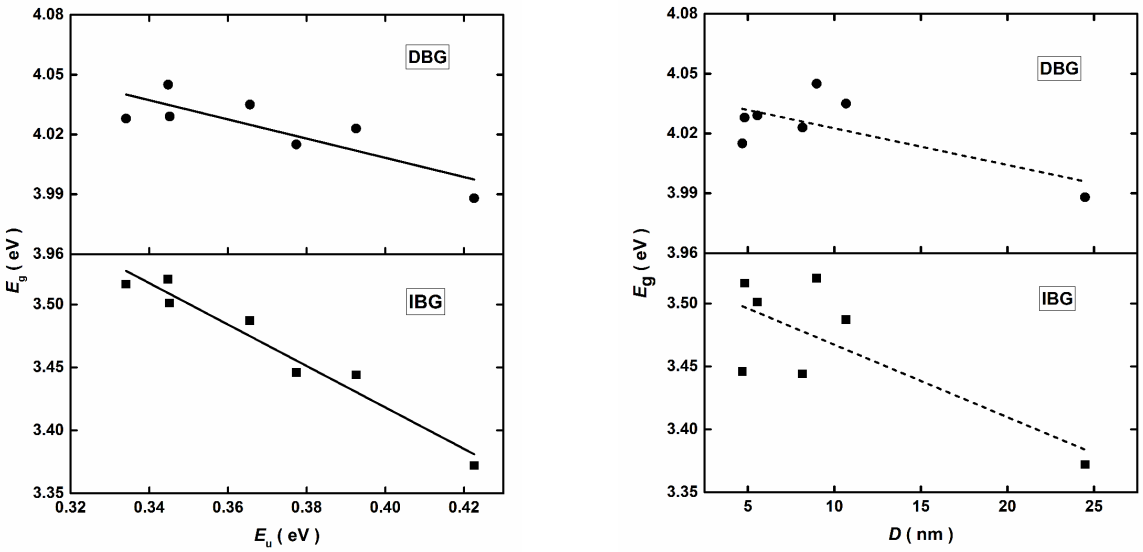

Fig 10. Correlation of band gap with (a) Urbach energy and (b) crystallite size in Ni_2O_3 thin films.

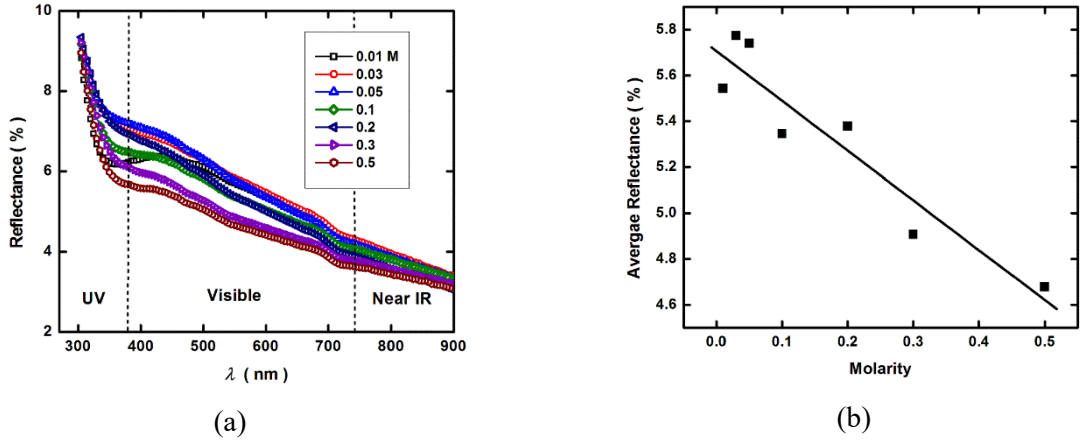

Fig 11. (a) Reflectance spectra of Ni_2O_3 films of various molarities in the wavelength range 270 – 900 nm.(b) Variation in the average reflectance of Ni_2O_3 thin films in the visible region as a function of the molarity.

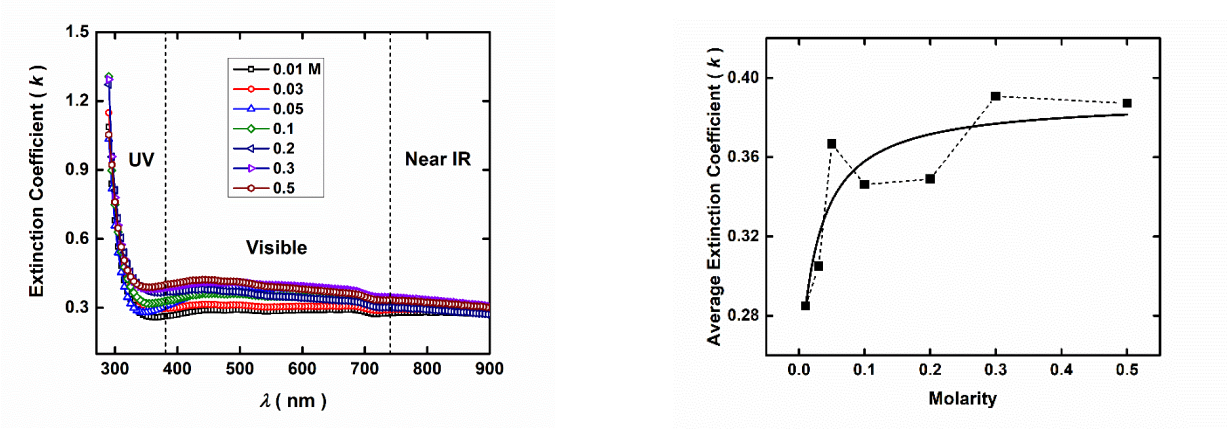

Fig 12. (a) Extinction coefficient (k) spectra of Ni_2O_3 thin films of various molarities in the wavelength range 270 – 900 nm. (b) Variation in the average extinction coefficient (*k*) of Ni_2O_3 thin films in the visible region as a function of molarity.

relation [20]:

$$\sigma_{op} = cn\alpha / 4\pi \quad (26)$$

where c stands for the speed of light, and other symbols have already been defined. The σ_{op} values calculated for Ni_2O_3 films (0.01 – 0.5 M) vis-à-vis photon energy $h\upsilon$ have been portrayed in Fig. 14a. For a given molar concentration, the rise in σ_{op} value with photon energy can be attributed to the fact that more electrons will be excited if the photon energy is higher [64]. Similar response for different materials has also been reported by various researchers [65, 66]. Average values of optical conductivity in the visible region (380 – 740 nm) vis-à-vis molarity have been plotted in Fig. 14b. A curve fitted to the data points is encompassed by following expression:

$$\sigma_{op}^{ave} = (2.930 \times 10^{15}) - (8.439 \times 10^{14})\exp(-48.452M) \quad (27)$$

with correlation factor r^2 = 0.846. An increasing trend of the average optical conductivity (σ_{op}^{ave}) with molarity is quite rapid in the low molarity range (0.01 – 0.05 M) and fairly moderate in the high molarity range (0.1 – 0.5 M). This trend is somewhat reminiscent of that portrayed in Fig 4b and Fig 12b for the average absorbance (A_{ave}) and average extinction coefficient (k_{ave}) in the visible region, respectively.

3.2.8 Dielectric Constant

Dielectric constant of any solid is a measure of its polarizability [67]. Since dielectric constant depends on the photon energy, it points to some interaction of electrons with phonons in solid. The complex dielectric constant, which depends on frequency, is given by $\varepsilon^* = \varepsilon_1 + i\varepsilon_2$, where $\varepsilon_1 = n^2 - k^2$ and $\varepsilon_2 = 2nk$. The first or real part (ε_1) is attributed to the slowing down phenomenon of the speed of light in solid and the second or imaginary part ($i\varepsilon_2$) pertains to dipole motion due to absorption of energy from electric field [20, 68]. The calculated values of ε_1 and ε_2 of the Ni_2O_3 thin films of various molar concentrations have been plotted against wavelength of incident photons in Fig 15a and Fig 15b, respectively. For a given wavelength, ε_1 is decreasing with the increase in molarity, and is minimum for 0.5 M thin film whereas ε_2 is increasing with the increase in molarity.

3.3 Surface Morphological Analysis

Figure 16 depicts the SEM micrographs (magnification × 3000) of Ni_2O_3 thin films (0.01 – 0.5 M) synthesized in the present work. One can notice random shape nanoparticles uniformly dispersed over the film surface. Moreover, with an increase in molarity the density of nanoparticles has also increased. The 3D images of the SEM micrographs given in Fig. 16 were obtained using the WSxM Nanotech software [69], and are given in Fig 17. This software can convert not only a SEM micrograph into its 3D image but also provides quantitative information about the topographical features of the image. The topographic histograms of the SEM images (Fig 16) obtained by WSxM Nanotech software [69] are shown in Fig 18. The height of the particles is given on the abscissa whereas the ordinate scale refers to the number of particles of a given height.

The quality of the smoothness of a thin film surface is described in terms of (i) average surface roughness R_a and (ii) root-mean-square surface roughness R_{rms}. These are defined as below:

$$R_a = \left(\frac{1}{N}\right)\sum_{i=1}^{N}(Z_i - Z_0) \quad (28)$$

$$R_{rms} = \left[\left(\frac{1}{N}\right)\sum_{i=1}^{N}(Z_i - Z_0)^2\right]^{\frac{1}{2}} \quad (29)$$

where Z_i is the height of a given particle, N is the total number of particles within the analyzed area, and Z_o is the average height of N particles [51]. Table 4 displays R_a and R_{rms} values obtained by WSxM Nanotech software [69] and the symbols

Table 4. Surface Roughness of Ni_2O_3 films

Molarity	RMS Roughness (µm)	Average Roughness (µm)
0.01	0.252	0.173
0.03	0.439	0.366
0.05	0.334	0.273
0.1	0.366	0.281
0.2	0.286	0.257
0.3	0.382	0.319
0.5	0.348	0.292

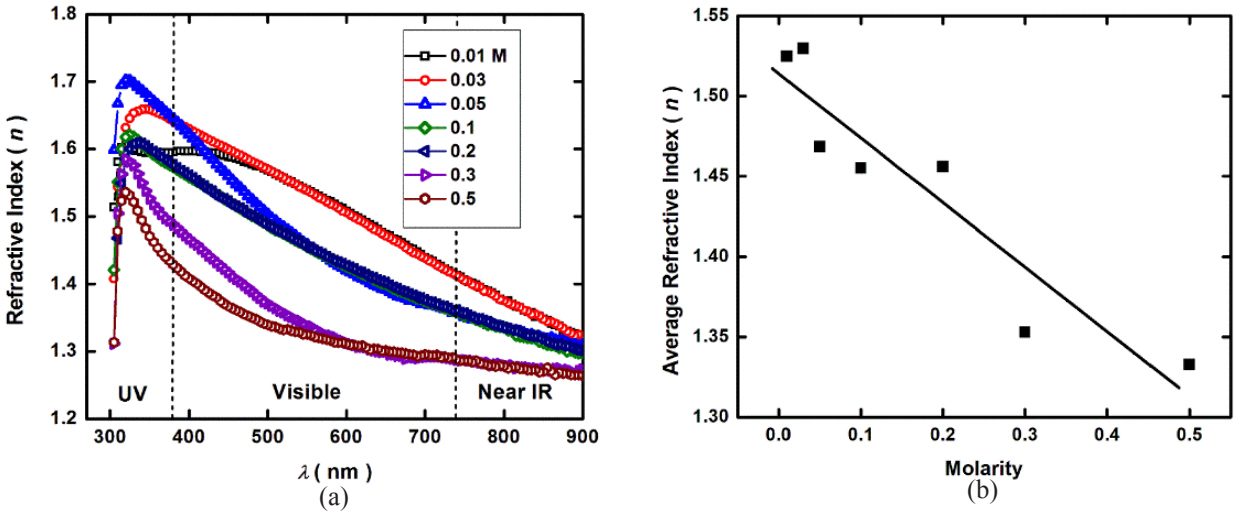

(a) (b)

Fig 13. (a) Refractive index spectra of Ni_2O_3 thin films of various molarities in the wavelength range 270 – 900 nm. (b) Variation in the average refractive index of Ni_2O_3 thin films in the visible region as a function of molarity.

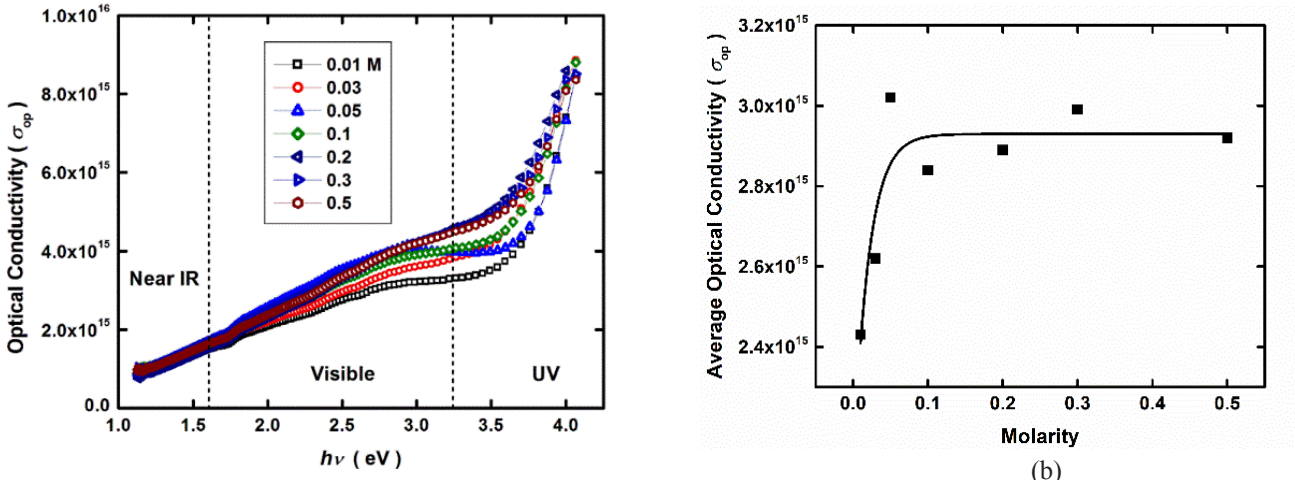

(a) (b)

Fig 14. (a) Optical conductivity spectra of Ni_2O_3 thin films of various molarities in the wavelength range 270 – 900 nm. (b) Variation in the average optical conductivity of Ni_2O_3 thin films in the visible region as a function of molarity.

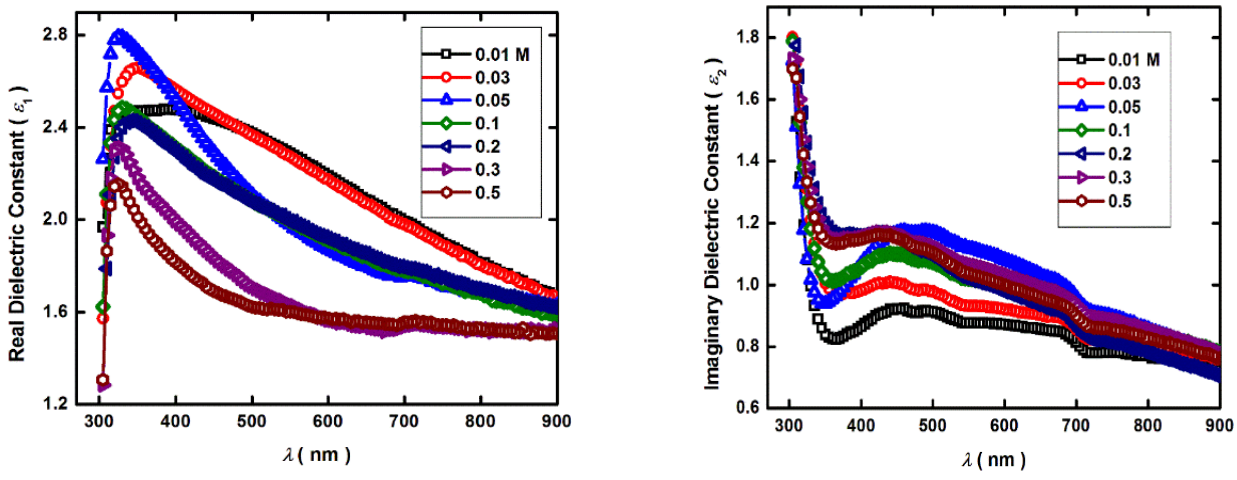

(a) (b)

Fig 15. Values of (a) the real part of dielectric constant and (b) the imaginary part of dielectric constant as a function of wavelength in the range 270 – 900 nm.

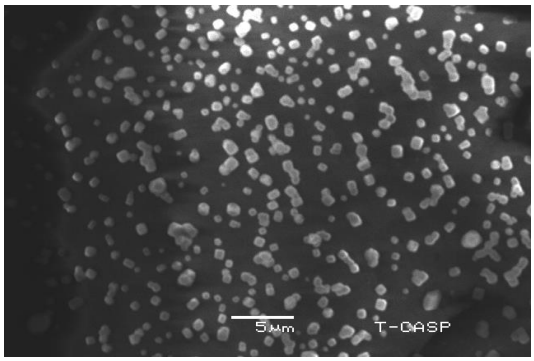

0.01 M

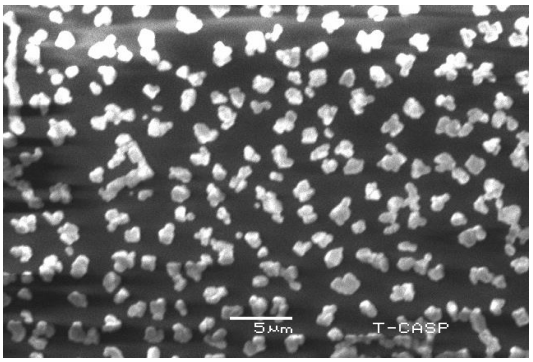

0.03 M

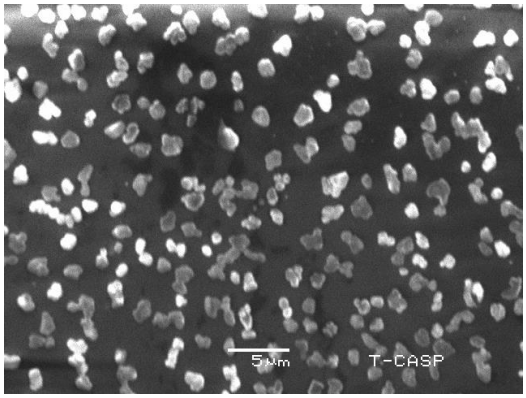

0.05 M

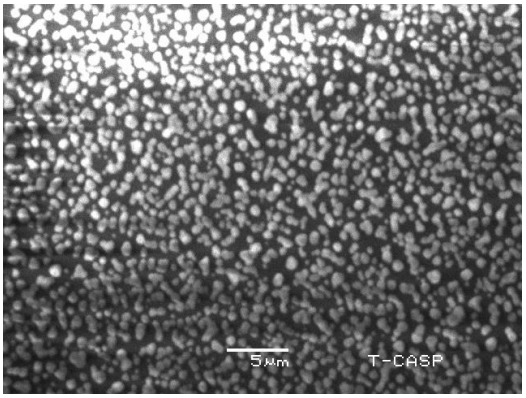

0.1 M

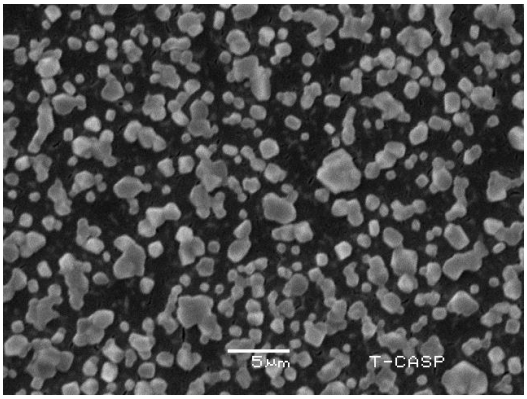

0.2 M

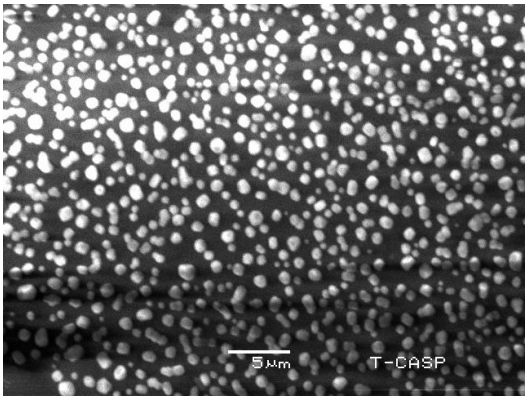

0.3 M

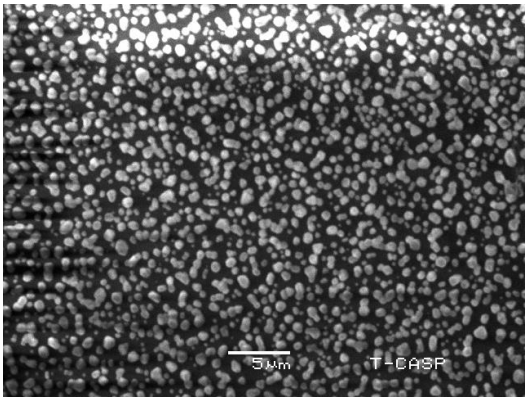

0.5 M

Fig 16. SEM micrographs of Ni_2O_3 films of various molarities in the range 0.01 – 0.5 M.

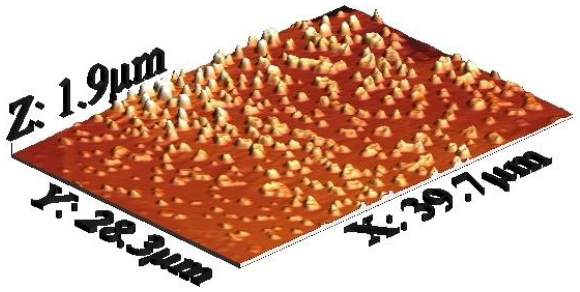

(a) 0.01 M

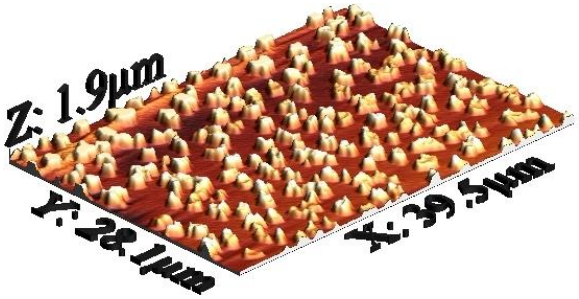

(b) 0.03 M

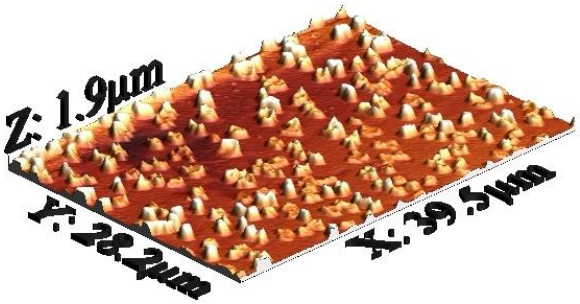

(c) 0.05 M

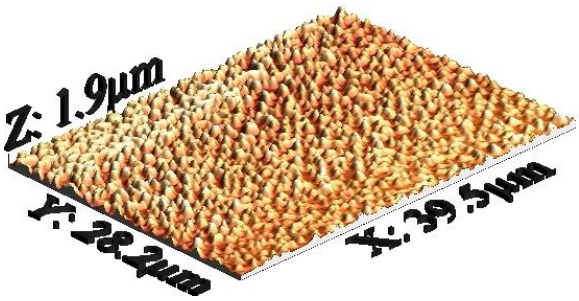

(d) 0.1 M

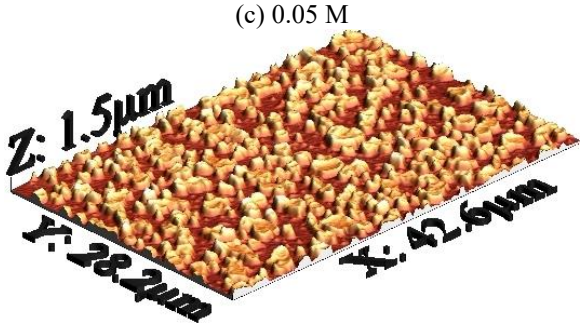

(e) 0.2 M

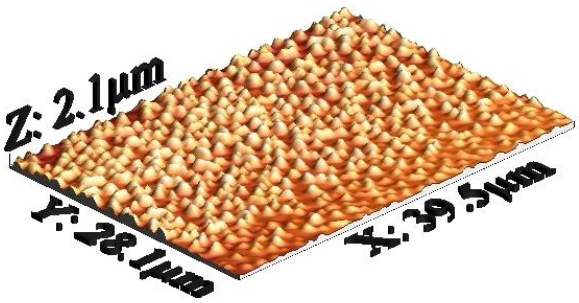

(f) 0.3 M

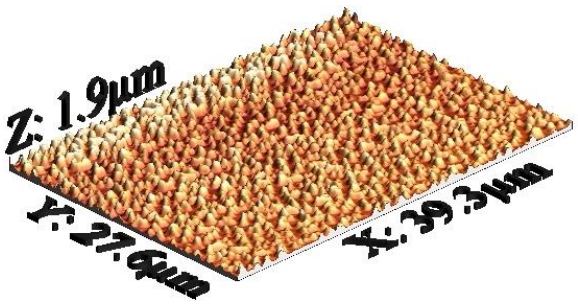

(g) 0.5 M

Fig 17. 3D images of SEM micrographs of Ni_2O_3 films depicted in **Fig 16.**

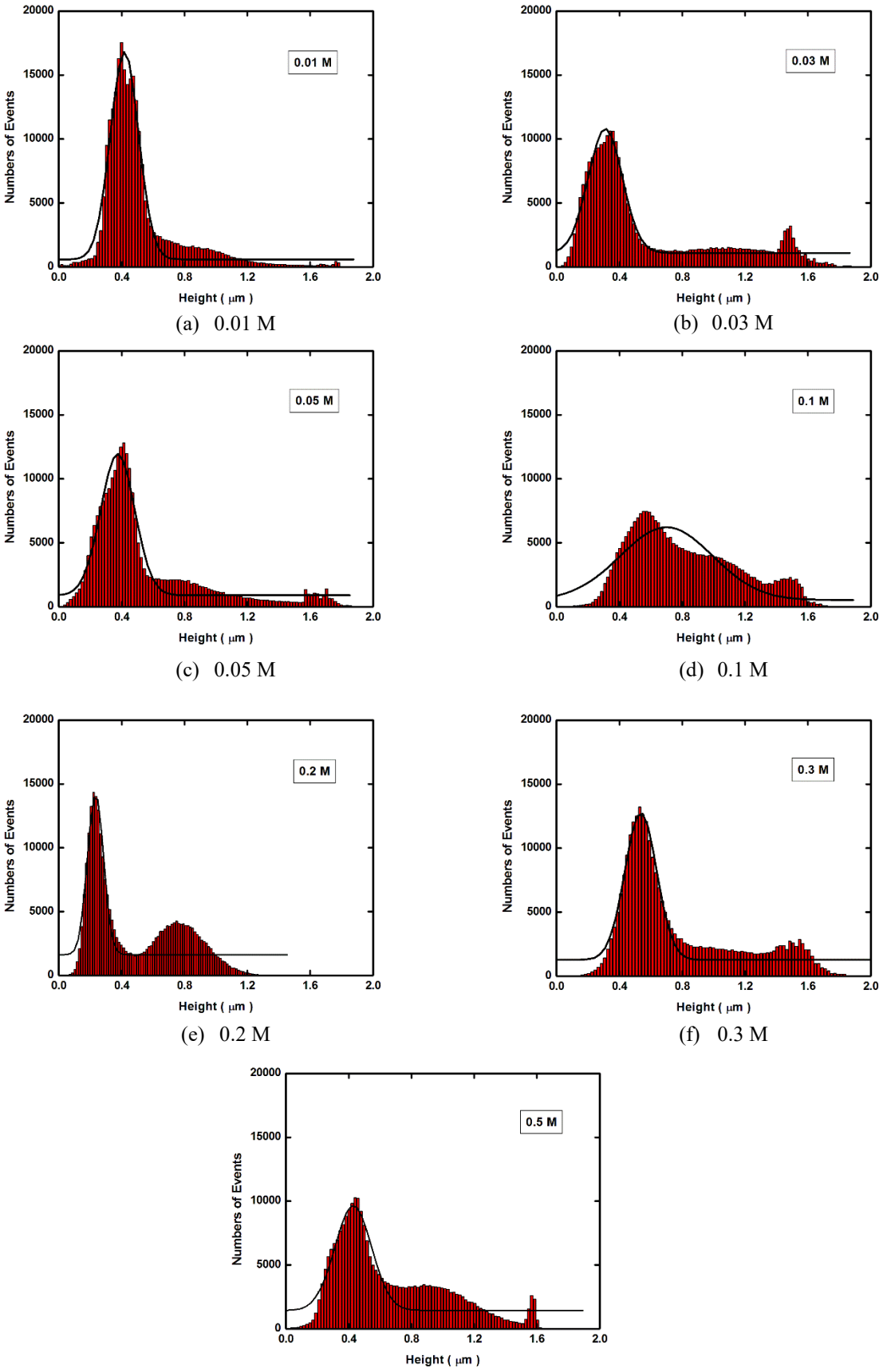

(a) 0.01 M (b) 0.03 M

(c) 0.05 M (d) 0.1 M

(e) 0.2 M (f) 0.3 M

(g) 0.5 M

Fig 18. Histograms of SEM micrographs of Ni_2O_3 films depicted in Fig 16.

in Fig 19 denote these values vis-à-vis molarity. It is observed that the surface roughness of the Ni_2O_3 films increases rapidly with molarity in the range 0.01 – 0.03 M (Rrms = 0.252 to 0.439 µm and Ra = 0.173 to 0.366 µm), and then it falls down to an intermediate level around which it undulates till 0.5M. The dash lines in the molarity range 0.05 – 0.5M represent average value 0.343 µm for Rrms and 0.284 µm for Ra. On comparison of Fig 19 with Fig. 4a, Fig 12b, and Fig 14b, it appears that surface roughness of the Ni_2O_3 films strongly exerts its influence on the absorbance, extinction coefficient, and optical conductivity of the films.

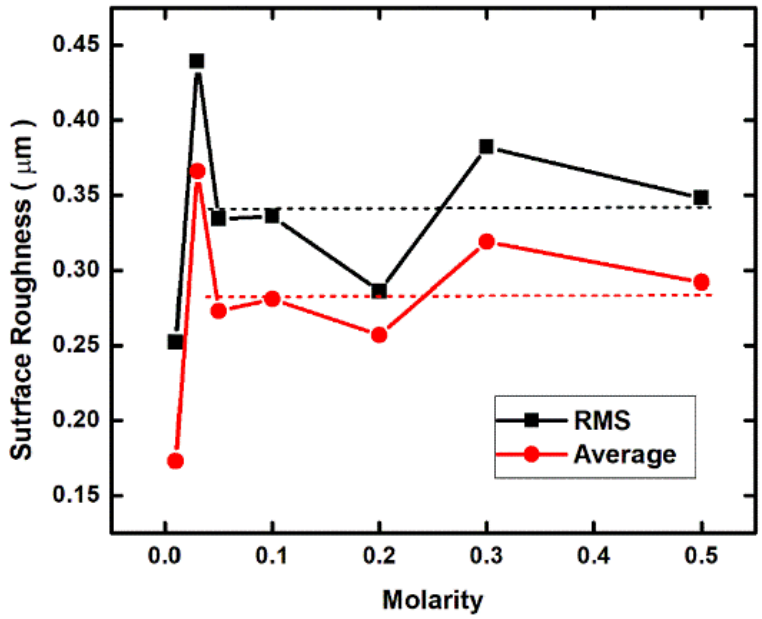

Fig 19. Surface roughness of Ni_2O_3 thin films as a function of molarity.

4. CONCLUSIONS

In the present study, surface runoff potential was Ni_2O_3 thin films with seven molar concentrations ranging from 0.01 – 0.5 M were deposited on pre-heated glass substrates employing spray pyrolysis technique. Characterization of the synthesized films lead us to the conclusions as follows.

1. Structure of the films was hexagonal with one major peak of (002) plane.
2. The peak intensity (87 – 777 cps) and crystallite size (4.7 – 24.5 nm) of (002) plane increased exponentially with the increase in molarity.
3. Both uniform and non-uniform lattice strains as well as stacking fault probability decreased linearly on increasing molarity.
4. Average values of optical absorbance (0.554 – 0.762), extinction coefficient (0.285 – 0.391), and optical conductivity (2.43 – 3.02) in the visible region (λ = 380 – 740 nm) increased rapidly with molarity in the low molarity range 0.01 – 0.05M and rather slowly in the high molarity range (0.1 – 0.5 M).
5. Both direct (3.99 – 4.045 eV) and indirect (3.37 – 3.52 eV) band gaps decreased whereas Urbach energy (0.33 – 0.42 eV) increased on increasing molarity.
6. Optical reflectance of the films (λ = 270 – 900 nm) was less than 10%. Average reflectance (4.677 – 5.774 %) in the visible region (λ = 380 – 740 nm) decreased linearly on increasing molarity.
7. The average refractive index (1.33 – 1.53) in the visible region decreased linearly with increase in molarity.
8. Surface morphology of the films consisted of random shape nanoparticles.
9. Average surface roughness of the films (0.173 – 0.366 µm) increased rapidly with molarity in the range 0.01 – 0.03 M, and then decreased to an intermediate level (0.284 µm) around which it undulated in the range 0.05 – 0.5 M.
10. Surface roughness of the films strongly exerts its influence on the absorbance, extinction coefficient, and optical conductivity of the

films.

5. ACKNOWLEDGEMENTS

Authors are grateful to Dr. Tousif Hussain (Centre for Advanced Studies in Physics, GC University, Lahore) for taking SEM micrographs of the specimens.

7. REFERENCES

1. D. S. Ginley, and C. Bright. Transparent Conducting Oxides. *MRS Bulletin* 25: 15 – 18 (2000).
2. P. P. Edwards, A. Porch, M. O. Jones, D. V. Morgan, and R. M. Perks. Basic materials physics of transparent conducting oxides. *Dalton Transactions* 19: 2995 – 3002 (2004).
3. T. J. Coutts, D. L. Young, and X. Li. Characterization of transparent conducting oxides. *MRS Bulletin* 25: 58 – 65 (2000).
4. K. H. L. Zhang, K. Xi, M. G. Blamire, and R. G. Egdell. P-type transparent conducting oxides. *Journal of Physics: Condensed Matter* 28: 383002 (2016).
5. M. Aftab, M. Z. Butt, D. Ali, F. Bashir, and Z. H. Aftab. Impact of copper doping in NiO thin films on their structure, morphology, and antibacterial activity against *Escherichia coli*. *Ceramics International* 46: 5037 – 5049 (2020).
6. J-M. Choi, and S. Im. Ultraviolet enhanced Si-photodetector using p-NiO films. *Applied Surface Science* 244: 435 – 438 (2005).
7. G. Bodurov, P. Stefchev, T. Ivanova, and K. Gesheva. Investigation of electrodeposited NiO films as electrochromic material for counter electrodes in "Smart Windows". *Materials Letters* 117: 270 – 272 (2014).
8. H. Ohta, M. Kamiya, T. Kamiya, M. Hirano, and H. Hosono. UV-detector based on pn-heterojunction diode composed of transparent oxide semiconductors, p-NiO/n-ZnO. *Thin Solid Films* 445: 317 – 321 (2003).
9. Y-M. Lee, C-H. Hsu, and H-W. Chen. Structural, optical, and electrical properties of p-type NiO films and composite TiO2/NiO electrodes for solid-state dye-sensitized solar cells. *Applied Surface Science* 255: 4658 – 4663 (2009).
10. J. Wang, P. Yang, X. Wei, and Z. Zhou. Preparation of NiO two-dimensional grainy films and their high-performance gas sensors for ammonia detection. *Nanoscale Research Letters* 10: 119 (2015).
11. X. Wen, X. Chen, N. Tian, J. Gong, J. Liu, M. H. Rümmeli, P. K. Chu, E. Mijiwska, and T. Tang. Nanosized carbon black combined with Ni_2O_3 as "universal" catalysts for synergistically catalyzing carbonization of polyolefin wastes to synthesize carbon nanotubes and application for supercapacitors. *Environmental Science & Technology* 48: 4048 – 4055 (2014).
12. S. Dey, S. Santra, A. Midya, P. K. Guha, and S. K. Ray. Synthesis of CuxNi(1-x)O coral like nanostructures and its application in design of re-usable toxic heavy metal ion sensor based on adsorption mediated electrochemical technique. *Environmental Science: Nano* 4:191 – 202 (2017).
13. S. Dey, S. Bhattacharjee, M. G. Chaudhuri, R. S. Bose, S. Halder, and C. K. Ghosh. Synthesis of pure nickel(III) oxide nanoparticles at room temperature for Cr(VI) ion removal. *RSC Advances* 5: 54717 – 54726 (2015).
14. W. F. Chen, and S. Y. Wu. The effect of temperature on the preparation of electrochromic nickel oxide by an electroless method. *Applied Surface Science* 253: 1907 – 1911 (2006).
15. W. F. Chen, S. Y. Wu, and Y. F. Ferng. The electrochromic properties of nickel oxide by chemical deposition and oxidization. *Materials Letters* 60: 790 – 795 (2006).
16. S. Hu, F. Li, and Z. Fan. The Synergistic Effect of nitrogen and Ni_2O_3 over TiO2 photocatalyst in the degradation of 2, 4, 6-trichlorophenol under visible light. *Bulletin of the Korean Chemical Society* 33: 4052 – 4058 (2012).
17. W. Zhao, W. Ma, C. Chen, J. Zhao, and Z. Shuai. Efficient degradation of toxic organic pollutants with Ni_2O_3/TiO2-xBx under visible irradiation. *Journal of the American Chemical Society* 126: 4782 – 4783 (2004).
18. N. A. Bakr, Z. T. Khodair, and A. M. Shano. Effect of aqueous solution molarity on structural and optical properties of Ni0.92Co0.08O thin films prepared by chemical spray pyrolysis method. *International Journal of Thin Films Science and Technology* 4: 111 – 119 (2015).
19. S. Sriram, and A. Thayumanavan. Structural, optical and electrical properties of NiO thin films prepared by low cost spray pyrolysis technique. *International Journal of Materials Science and Engineering* 1: 118 – 121 (2013).
20. K. S. Usha, R. Sivakumar, and C. Sanjeeviraja. Optical constants and dispersion energy parameters of NiO thin films prepared by radio frequency magnetron sputtering technique. *Journal of Applied*

Physics 114: 123501 (2013).

21. S. Dendouga, S. Benramache, and S. Lakel. Influence of film thickness on optical and electrical properties of nickel oxide (NiO) thin films. Journal of Chemistry and Materials Research 5: 78̃84 (2016).
22. B. A. Reguig, A. Khelil, L. Cattin, M. Morsli, and J. C. Berne`de. Properties of NiO thin films deposited by intermittent spray pyrolysis process. *Applied Surface Science* 253: 4330 – 4334 (2007).
23. H. Kamal, E. K. Elmaghraby, S. A. Ali, and K. Abdel-Hady. The electrochromic behavior of nickel oxide films sprayed at different preparative conditions. *Thin Solid Films* 483: 330 – 339 (2005).
24. S. A. Mahmoud, S. Alshomer, and M. A. Tarawnh. Structural and optical dispersion characterization of sprayed nickel oxide thin films. *Journal of Modern Physics* 2: 1178 – 1186 (2011).
25. L. Cattin, B. A. Reguig, A. Khelil, M. Morsli, K. Benchouk, and J. C. Berne`de. Properties of NiO thin films deposited by chemical spray pyrolysis using different precursorr solutions. *Applied Surface Science* 254: 5814 – 5821 (2008).
26. P. S. Aggarwal, and A. Goswami. An Oxide of tervalent nickel. *Journal of Physical Chemistry* 65: 2105 (1961).
27. M. Z. Butt, D. Ali, M. Aftab, and M. U. Tanveer. Surface topography and structure of laser-treated high-purity zinc. *Surface Topography: Metrology and Properties* 3: 035002 (2015).
28. D. Ali, and M. Z. Butt. Structural characteristics and inverse Hall–Petch relation in high-purity nickel irradiated with nanosecond infrared laser pulses. *Physica B: Condensed Matter* 444: 77 – 84 (2014).
29. B. D. Cullity, and S. R. Stock. *Elements of X-ray Diffraction*. 3rd edition, Prentice-Hall, New York (2001).
30. M. Z. Butt, F. Bashir, and S. Arooj. Effect of UV laser irradiation on the hardness and structural parameters of Ag_xPd_{1-x} ($0.4 \leq x \leq 0.6$) alloys. *Applied Surface Science* 259: 740 – 746 (2012).
31. B. E. Warren, and E. P. Warekois. Stacking faults in cold worked alpha-brass. *Acta Metallurgica* 3: 473 – 479 (1955).
32. D. Ali, M. Z. Butt, B. Arif, A. A. Al-Ghamdi, and F. Yakuphanoglu. The role of Al, Ba, and Cd dopant elements in tailoring the properties of c-axis oriented ZnO thin films. *Physica B: Condensed Matter* 506: 83 – 93 (2017).
33. A. R. Balu, V. S. Nagarethinam, N. Arunkumar, and M. Suganya. Nanocrystalline NiO thin films prepared by a low cost simplified spray technique using perfume atomizer. *Journal of Electron Devices* 13: 920 – 930 (2012).
34. C. Mrabet, M. B. Amor, A. Boukhachem, M. Amlouk, and T. Manoubi. Physical properties of La-doped NiO sprayed thin films for optoelectronic and sensor applications. *Ceramics International* 42:5963 – 5978 (2016).
35. F. S. Hashim, and N. A. Sami. Effect of Zn doping on structural and some optical studies of nano NiO films prepared by sol – gel technique. *International Letters of Chemistry Physics and Astronomy* 53: 31 – 40 (2015).
36. J. Tauc. *Amorphous and liquid semiconductors*. Plenum Press London and New York (1974).
37. H. Aydin, S. A. Mansour, C. Aydin, A. A. Al-Ghamdi, O. A. Al-Hartomy, F. El-Tantawy, and F. Yakuphanoglu. Optical properties of nanostructure boron doped NiO thin films. *Journal of Sol-Gel Science and Technology* 64: 728 – 733 (2012).
38. S. M. Reda, and S. M. Al-Ghannam. Synthesis and electrical properties of polyaniline composite with silver nanoparticles. *Advances in Materials Physics and Chemistry* 2, 75 – 81 (2012).
39. S. Adachi. *Optical properties of crystalline and amorphous semiconductors*. Kluwer, Boston (1999).
40. H. Kamal, E. K. Elmaghraby, S. A. Ali, and K. Abdel-Hady. Characterization of nickel oxide films deposited at different substrate temperatures using spray pyrolysis. *Journal of Crystal Growth* 262: 424 – 434 (2004).
41. D. P. Joseph, M. Saravanan, B. Muthuraaman, P. Renugambal, S. Sambasivam, S. P. Raja, P. Maruthamuthu, and C. Venkateswaran. Spray deposition and characterization of nanostructured Li doped NiO thin films for application in dye-sensitized solar cells. *Nanotechnology* 19: 485707 (2008).
42. P. S. Patil, and L. D. Kadam. Preparation and characterization of spray pyrolyzed nickel oxide (NiO) thin films. *Applied Surface Science* 199: 211 – 221 (2002).
43. T. Chtouki, L. Soumahoro, B. Kulyk, H. Bougharraf, B. Kabouchi, H. Erguig, and B. Sahraoui. Comparison of structural, morphological, linear and nonlinear optical properties of NiO thin films elaborated by spin-coating and spray pyrolysis. *Optik* 128: 8 – 13 (2017).
44. S. R. Nalage, M. A. Chougule, S. Sen, P. B. Joshi, and V. B. Patil. Sol–gel synthesis of nickel oxide thin films and their characterization. *Thin Solid Film*

520: 4835 – 4840 (2012).
45. V. Patil, S. Pawar, M. Chougule, P. Godse, R. Sakhare, S. Sen, and P. Joshi. Effect of annealing on structural, morphological, electrical and optical studies of nickel oxide thin films. *Journal of Surface Engineered Materials and Advanced Technology* 1: 35 – 41 (2011).
46. G. Turgut, E. Sonmeza, and S. Duman. Determination of certain sol-gel growth parameters of nickel oxide films. *Ceramics International* 41: 2976 – 2989 (2015).
47. S. A. Mahmoud, A. A. Akl, H. Kamal, and K. Abdel-Hady. Opto-structural, electrical and electrochromic properties of crystalline nickel oxide thin films prepared by spray pyrolysis. *Physica B* 311: 366 – 375 (2002).
48. M. Anwar, and C. A. Hogarth. Structural investigations and colour centres in MoO3 films deposited by vacuum evaporation, *International Journal of Electronics* 67: 567 – 576 (1989).
49. U. Chaitra, D. Kekuda, and K. Mohan Rao. Dependence of solution molarity on structural, optical and electrical properties of spin coated ZnO thin films. *Journal of Materials Science: Materials in Electronics* 27: 7614 – 7621 (2016).
50. F. Urbach. The long-wavelength edge of photographic sensitivity and of the electronic absorption of solids. *Physical Review* 92: 1324 (1953).
51. D. Ali, M. Z. Butt, B. Arif, A. G. Al-Sehemi, A. A. Al-Ghamdi, and F. Yakuphanoglu. Li induced enhancement in c-axis orientation and its effect on structural, optical, and electrical properties of ZnO thin films. *Materials Research Express* 4: 026405 (2017).
52. K. C. Lalithambika, K. Shanthakumari, and S. Sriram. Optical Properties of CdO Thin Films deposited by Chemical Bath Method. *International Journal of ChemTech Research* 6: 3071 – 3077 (2014).
53. S. Benramache, and M. Aouassa. Preparation and characterization of p-type semiconducting NiO thin Films Deposited by Sol-Gel Technique. *Journal of Chemistry and Material Research* 5: 119 – 122 (2016).
54. A. J. R. Mary, and S. Arumugam. Structural and optical studies of molarity based ZnO thin films. *Nano Hybrids and Composites* 17: 140 – 148 (2017).
55. F. Z. Boutebakh, A. Beloucif, M. S. Aida, A. Chettah, and N. Attaf. Zinc molarity effect on Cu2ZnSnS4 thin film properties prepared by spray pyrolysis. *Journal of Materials Science: Materials in Electronics* 29: 4089 – 4095 (2018).
56. D. Ali, M. Z. Butt, I. Muneer, F. Bashir, and M. Saleem. Correlation between structural and optoelectronic properties of tin doped indium oxide thin films. *Optik* 128: 235 – 246 (2017).
57. S. Riaz, S. Rehman, M. Abutalib, and S. Naseem. Structural, Optical, and dielectric properties of aluminum oxide nanofibers synthesized by a lower-temperature sol–gel approach. *Journal of Electronic Materials* 45: 5185 – 5197 (2016).
58. S. Benramache and B. Benhaoua, Influence of Urbach energy with solution molarity on the electrical conductivity in undoped ZnO thin films, *Journal of Nano- and Electronic Physics* 8: 02025 (2016).
59. A. Hafdallah, F. Yanineb, M.S. Aida, and N. Attaf. In doped ZnO thin films. *Journal of Alloys and Compounds* 509: 7267 – 7270 (2011).
60. M. Jlassi, I. Sta, M. Hajji, and H. Ezzaouia. Synthesis and characterization of nickel oxide thin films deposited on glass substrates using spray pyrolysis. *Applied Surface Science* 308: 199 – 205 (2014).
61. M. Vigneshkumar, S. S. Muthulakshmi, J. Pandiarajan, A. Saranya, and N. Prithivikumaran. Structural and optical properties of nanocrystalline nickel oxide thin film by spray pyrolysis technique. *International Journal of Technical Research and Applications* 38: 52 – 56 (2016).
62. A. Alshahrie, I. S. Yahia, A. Alghamdi, and P. Z. A. Hassan. Morphological, stuctural and optical dispersion parameters of Cd-doped NiO nanostructure thin film. *Optik* 127: 5105 – 5109 (2016).
63. C. F. K. Lingshirn, Semiconductor *Optics*, 4th edition, Springer-Verlag, Berlin Heidelberg (2012).
64. F. Yakuphanoglu, A. Cukurovali, and I. Yilmaz. Refractive index and optical absorption properties of thecomplexes of a cyclobutane containing thiazolyl hydrazone ligand. *Optical Materials* 27: 1363 – 1368 (2005).
65. A. E. Korashya, H. E. Zahed, and M. Radwan. Optical studies of [N(CH3)4]2CoCl4, [N(CH3)4]2MnCl4 single crystals in the normal paraelectric phase. *Physica B: Condensed Matter* 334: 75 – 81 (2003).
66. M. M. Wakkad, E. K. Shokr, and S. H. Mohamed. Optical and calorimetric studies of Ge-Sb-Se glasses. *Journal of Non-Crystalline Solids* 265: 157 – 166 (2000).
67. A. B. Khatibani, and S. M. Rozati. Optical and morphological investigation of aluminum and nickel

oxide composite films deposited by spray pyrolysis method as a basis of solar thermal absorber. *Bulletin of Materials Science* 38: 319 – 326 (2015).

68. P. Sharma, V. Sharma, and S. C. Katyal. Variation of optical constants in $Ge_{10}Se_{60}Te_{30}$ thin film, *Chalcogenide Letters* 3: 73 – 79 (2006).
69. I. Horcas, R. Fernández, J. M. G. Rodríguez, J. Colchero, J. G. Herrero, and A. M. Baro. WSXM: A software for scanning probe microscopy and a tool for nanotechnology. *Review of Scientific Instruments* 78: 013705 (2007).